ADVANCED MATERIALS
www.advmat.de

# Electrically Confined Electroluminescence of Neutral Excitons in $WSe_2$ Light-Emitting Transistors

*June-Chul Shin, Jae Hwan Jeong, Junyoung Kwon, Yeon Ho Kim, Bumho Kim, Seung-Je Woo, Kie Young Woo, Minhyun Cho, Kenji Watanabe, Takashi Taniguchi, Young Duck Kim, Yong-Hoon Cho, Tae-Woo Lee, James Hone, Chul-Ho Lee, and Gwan-Hyoung Lee**

**Monolayer transition metal dichalcogenides (TMDs) have drawn significant attention for their potential in optoelectronic applications due to their direct band gap and exceptional quantum yield. However, TMD-based light-emitting devices have shown low external quantum efficiencies as imbalanced free carrier injection often leads to the formation of non-radiative charged excitons, limiting practical applications. Here, electrically confined electroluminescence (EL) of neutral excitons in tungsten diselenide ($WSe_2$) light-emitting transistors (LETs) based on the van der Waals heterostructure is demonstrated. The $WSe_2$ channel is locally doped to simultaneously inject electrons and holes to the 1D region by a local graphene gate. At balanced concentrations of injected electrons and holes, the $WSe_2$ LETs exhibit strong EL with a high external quantum efficiency (EQE) of ≈8.2 % at room temperature. These experimental and theoretical results consistently show that the enhanced EQE could be attributed to dominant exciton emission confined at the 1D region while expelling charged excitons from the active area by precise control of external electric fields. This work shows a promising approach to enhancing the EQE of 2D light-emitting transistors and modulating the recombination of exciton complexes for excitonic devices.**

## 1. Introduction

Transition metal dichalcogenides (TMDs) and their van der Waals (vdW) heterostructures have been considered promising platforms for next-generation optoelectronics because the TMDs have shown large binding energies of excitons and strong light–matter interactions with near-unity photoluminescence (PL) quantum yield (QY) in a monolayer limit due to broken-inversion symmetry.[1–7] The exceptional properties of the TMDs have facilitated the development of exotic optoelectronic quantum devices that exhibit unique capabilities, such as chiral light emission, excitonic complexes, and high-temperature exciton condensation, that have not been observed in conventional bulk materials.[8–12] Despite the great potential of the monolayer TMDs, the low external quantum efficiency (EQE) of TMD-based light-emitting devices and control of exciton complexes are major challenges to be addressed for practical applications.[13–18]

Enhancing the EQE of TMD-based light-emitting devices necessitates the fulfillment of two main prerequisites: First, it is essential to elevate the efficacy of radiative electron–hole (e–h) recombination within the TMDs. Second, achieving efficient and balanced injection of charge carriers into the TMDs is of paramount importance for facilitating effective light emission.[19] However, it is challenging to achieve both

J.-C. Shin, J. H. Jeong, S.-J. Woo, T.-W. Lee, G.-H. Lee
Department of Materials Science and Engineering
Seoul National University
Seoul 08826, Republic of Korea
E-mail: gwanlee@snu.ac.kr

J. Kwon
Department of Material Science and Engineering
Yonsei University
Seoul 03722, Republic of Korea

Y. H. Kim
KU-KIST Graduate School of Converging Science and Technology
Korea University
Seoul 02841, Republic of Korea

The ORCID identification number(s) for the author(s) of this article can be found under https://doi.org/10.1002/adma.202310498

DOI: 10.1002/adma.202310498

B. Kim
Department of Physics and Astronomy
University of Pennsylvania
Philadelphia, PA 19104, USA

K. Y. Woo, Y.-H. Cho
Department of Physics
Korea Advanced Institute of Science and Technology
Daejeon 34141, Republic of Korea

M. Cho, Y. D. Kim
Department of Physics and Department of Information Display
Kyung Hee University
Seoul 02447, Republic of Korea

K. Watanabe
Research Center for Electronic and Optical Materials
National Institute for Materials Science
1-1 Namiki, Tsukuba 305-0044, Japan

 

conditions simultaneously. Facilitating effective carrier injection into the emission layer requires elevated doping concentrations using methods, such as electrostatic or chemical doping, aiming to decrease the Schottky barrier height.[20] However, these increased doping levels in TMDs lead to the creation of exciton complexes, like charged excitons, predominantly contributing to non-radiative recombination.[6] This compromise limits the feasible doping range as a viable approach for carrier injection, necessitating the exploration of alternative injection mechanisms that enable effective carrier injection without generating excessive charge populations.

Here, we demonstrate electrically confined electroluminescence of neutral excitons in tungsten diselenide ($WSe_2$) LETs based on the vdW heterostructure consisting of $WSe_2$ (channel), graphene (electrodes and gate), and hexagonal boron nitride (hBN, dielectric). To achieve highly efficient light emission in the gate-tunable light-emitting transistors (LETs), we used $WSe_2$ as an emitting layer due to its ambipolar transport properties, direct bandgap, and high QY at room temperature.[7,21–25] Through the utilization of monolayer graphene as the gate-tunable source and drain electrodes with vdW contacts, we effectively mitigated Fermi level pinning and successfully attained appropriate band alignment for ambipolar transport within the $WSe_2$.[26–28] By electrically modulating gate and drain bias, our $WSe_2$ LETs selectively injected charge carriers of electrons and holes into $WSe_2$ from the respective graphene electrodes and effectively regulated the movement of these injected charges by modulating the barrier height at the $WSe_2$ homojunction, resulting in reconfigurable electrical transport properties. By balancing the densities of injected electrons and holes, we achieved strong EL with a high EQE of ≈8.2% at room temperature. The EL measurements revealed that neutral excitons dominantly contribute to the strong EL due to the confinement of neutral excitons within the 1D region facilitated by the in-plane electric field created by the local graphene gate and the expulsion of charged excitons from the 1D region by the charge interaction.

## 2. Results and Discussion

**Figure 1a** illustrates the $WSe_2$ LETs consisting entirely of 2D materials. We used double gates of graphene and Si to electrically confine the neutral excitons in the 1D region of $WSe_2$. To fabricate the devices, exfoliated flakes were stacked layer-by-layer using a dry pick-up transfer method.[29] The hBN-encapsulated monolayer $WSe_2$ FETs with the graphene contacts showed ambipolar transport characteristics (Figure S1, Supporting Information), which is in contrast to the monolayer $WSe_2$ FETs on a $SiO_2$/Si substrate with metal electrodes that exhibit only p-type conductance.[30,31] For local gating, the graphene flake was aligned precisely to overlap half of monolayer $WSe_2$. After transferring two monolayer graphene flakes for source and drain electrodes, the whole stack was encapsulated with the hBN because the hBN encapsulation can neutralize the doping level of TMDs and improve their optical and electrical properties.[32–34] Note that the $WSe_2$ used in this work was grown by the flux method, which is known as a method to synthesize high-quality 2D crystals with low defect density (Figure S2, Supporting Information).[35] After the transfer, the stack was annealed at 300 °C in a forming gas of hydrogen and argon for 3 h to remove residual bubbles between the stacked layers.[36] Raman and PL maps of the stacked sample show that the $WSe_2$ is in conformal contact with graphene electrodes (Figure S3, Supporting Information). Since the stacked sample of $WSe_2$ and graphene are embedded in the hBN, we used the graphene etch stop technique to form the via contacts to the embedded graphene electrodes, as described in our previous report.[37,38] The stacked sample was patterned by e-beam lithography and exposed to $XeF_2$ gas to etch the top hBN (hBN1), followed by metal deposition. There were no contamination and cracks in the devices, indicating the clean interfaces in the vdW heterostructure (see Figure S4, Supporting Information, for the fabrication process). As shown in the energy band diagram of Figure 1c, the Fermi energy levels of two graphene electrodes and the band offset of $WSe_2$ can be separately modulated by double gates of graphene and Si. By controlling the contact barrier heights at graphene–$WSe_2$ interfaces, two graphene electrodes can selectively inject electrons and holes into the $WSe_2$, respectively. Then, injected electrons and holes emit light through e–h recombination in the 1D region of $WSe_2$.

The double gate structure in the $WSe_2$ LET is crucial for the simultaneous modulation of injection and transport of both electrons and holes, unlike conventional ambipolar FETs with a single gate configuration that can transport only one type of charged carrier at a specific gate voltage. To validate gate-tunable carrier injection and transport in the $WSe_2$ LETs, we manipulated gate voltages of graphene ($V_{GG}$) and Si ($V_{BG}$) gates, as shown in **Figure 2**. Depending on the applied gate voltages of $V_{GG}$ and $V_{BG}$, the $WSe_2$ LET can reconFigure the polarity of transfer characteristics between n-type and p-type modes within a single $WSe_2$ channel, as shown in Figure 2a,b. When the Si back gate is biased at 60 V for n-type mode, the Fermi energy level of graphene source contact (Gr (S)) shifts close to the conduction band of $WSe_2$. Simultaneously, the conduction band of $WSe_2$ is bent down, resulting in efficient electron injection from Gr (S) to $WSe_2$, as illustrated in Figure 2c. At $V_{DS}$ = 0.5 V, $WSe_2$ LET exhibits n-type switching behavior with no noticeable hysteresis, consistent with previous reports.[39] This behavior can be attributed to the modulated transport of injected electrons by the energy barrier of $WSe_2$ homojunction through sweeping $V_{GG}$ (see Figure 2c(i),(ii)). Meanwhile, at a larger drain bias of $V_{DS}$ = 2 V, the transfer curve exhibited ambipolar transport behavior with a higher on-current compared to $V_{DS}$ = 0.5 V. Under positive voltage conditions of $V_{GG,}$ injected electrons from Gr (S) transport across the energy barrier at the $WSe_2$ homojunction (Figure 2c(ii)). At $V_{GG}$ = −6 V, the current increases owing to

T. Taniguchi
Research Center for Materials Nanoarchitectonics
National Institute for Materials Science
1-1 Namiki, Tsukuba 305-0044, Japan
J. Hone
Department of Mechanical Engineering
Columbia University
New York, NY 10027, USA
C.-H. Lee
Department of Electrical and Computer Engineering
Seoul National University
Seoul 08826, Republic of Korea

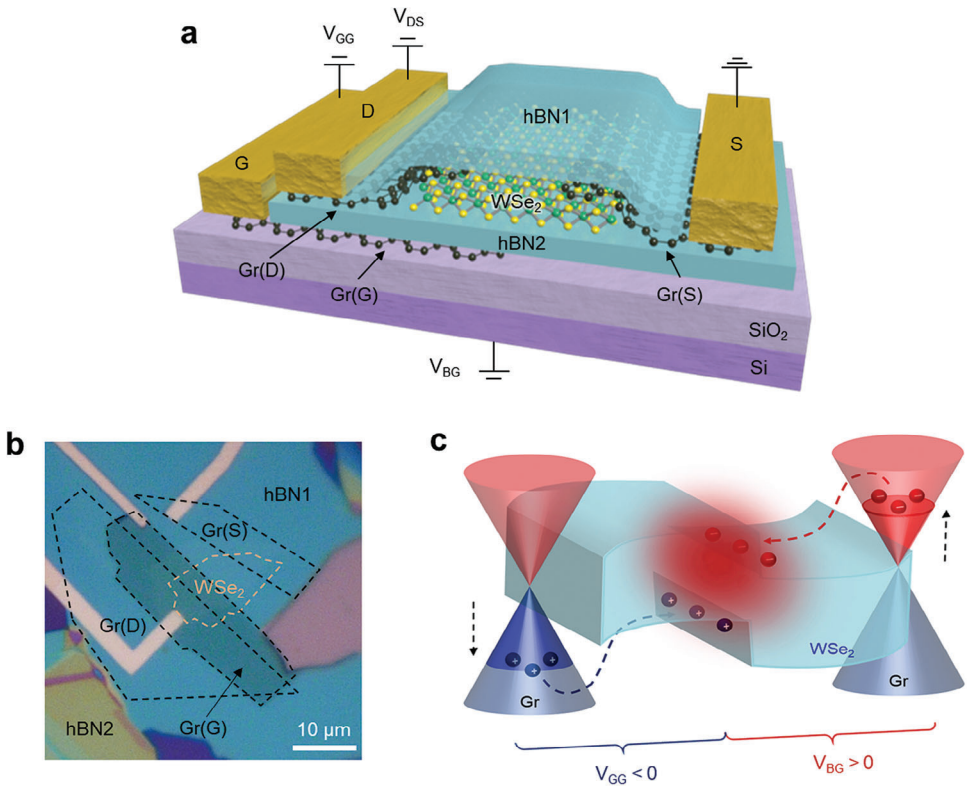


**Figure 1.** Device geometry and working principle of $WSe_2$ LET. a) Schematic illustration of 1L $WSe_2$ LET with 1L graphene contact encapsulated by hBN. $WSe_2$ LET has double gates of graphene and silicon gates. b) Optical image of the fabricated device. A portion of 1L $WSe_2$ is overlapped by the graphene gate. c) Band diagrams of the device at electroluminescence operation. The double gates can modulate individual regions of the divided $WSe_2$ layer, leading to injecting electrons or holes from graphene into the $WSe_2$ layer and transporting charge carriers in the $WSe_2$ layer. Light emission occurs in the 1D region between the p–n junction in a $WSe_2$ layer due to the e–h recombination of transported carriers.

the recombination of electrons and holes that are simultaneously injected from corresponding graphene contacts (Figure 2c(iii)). Conversely, when a negative gate voltage of $V_{GG} = -6$ V is applied for p-type operation, holes can be injected from the Gr (D) into the $WSe_2$ layer, leading to p-type transport (Figure S5, Supporting Information). These results indicate that our device can efficiently control both the selective injection of charge carriers and the transport of injected carriers through $WSe_2$.

Because of modulation of charge injection and local doping, the p–n homojunction in the $WSe_2$ shows rectifying behaviors in the output curves of **Figure 3a** (green dots at $V_{BG} = 60$ V and $V_{GG} = -6$ V and blue dots at $V_{BG} = -60$ V and $V_{GG} = 6$ V). The increase in forward bias current is attributed to the elevated recombination probability of injected electrons and holes from corresponding graphene electrodes at the 1D region of $WSe_2$. Therefore, when $V_{DS}$ was applied at 3 V at $V_{BG} = 60$ V and $V_{GG} = -6$ V, a strong EL peak was observed through the e–h recombination at the 1D region, which is similar to the PL spectrum of $WSe_2$, as shown in Figure 3b. This correspondence indicates that the EL at 1.65 eV originates from the e–h recombination across the direct bandgap of $WSe_2$. As estimated, the EL was clearly observed at the 1D region of $WSe_2$, as shown in the optical microscopic image of Figure 3c. Our photocurrent measurements also show that the photocurrent predominantly generates at the 1D region (Figure S6, Supporting Information). This indicates that the excitons generated by a laser can be dissociated into free carriers at the p–n junction owing to a built-in electric field.[20,40] In addition, we observed long EL retention over ≈$10^4$ s, indicating high stability of the $WSe_2$ LETs (Figure S7, Supporting Information).

To investigate the electrical tunability of the $WSe_2$ LETs, we measured the EL and EQE by varying drain bias and gate voltages in **Figure 4**. As the $V_{DS}$ increased (current density increases in the output curve in Figure 3a) at fixed gate voltages of $V_{BG} = 60$ V and $V_{GG} = -8$ V, the EL intensity increased with no EL peak shift as shown in Figure 4a. The EL intensity monotonically increased with the $V_{DS}$ owing to the effective injection of electrons and holes over a reduced contact barrier, reaching a high EQE of ≈5.3% at $V_{DS} = 2.5$ V at room temperature (Figure 4b and Figure S8, Supporting Information). The EQEs of the $WSe_2$ LETs were extracted using the method described in other reports[17,20] (see Note S1 and Figure S9, Supporting Information). At $V_{DS} > 2.5$ V, the EQE decreased due to non-radiative recombination paths, such as exciton–exciton annihilation at high exciton concentration.[20] To modulate the density of injected electrons, we measured the EL and EQE by varying the $V_{BG}$ at fixed $V_{GG} = -8$ V and $V_{DS} = 2.5$ V (Figure 4c,d). In this condition, the density of injected holes is fixed and more electrons are injected into the $WSe_2$ owing to reduced contact barrier by increasing the $V_{BG}$. As a result, the EL increased with $V_{BG}$, maintaining the EL peak position at 1.65 eV, as shown in Figure 4c. Similarly, we also observed an increase in the EL by varying $V_{GG}$ at fixed $V_{BG}$ and $V_{DS}$ due to the lowered contact barrier for hole injection (Figure S10,

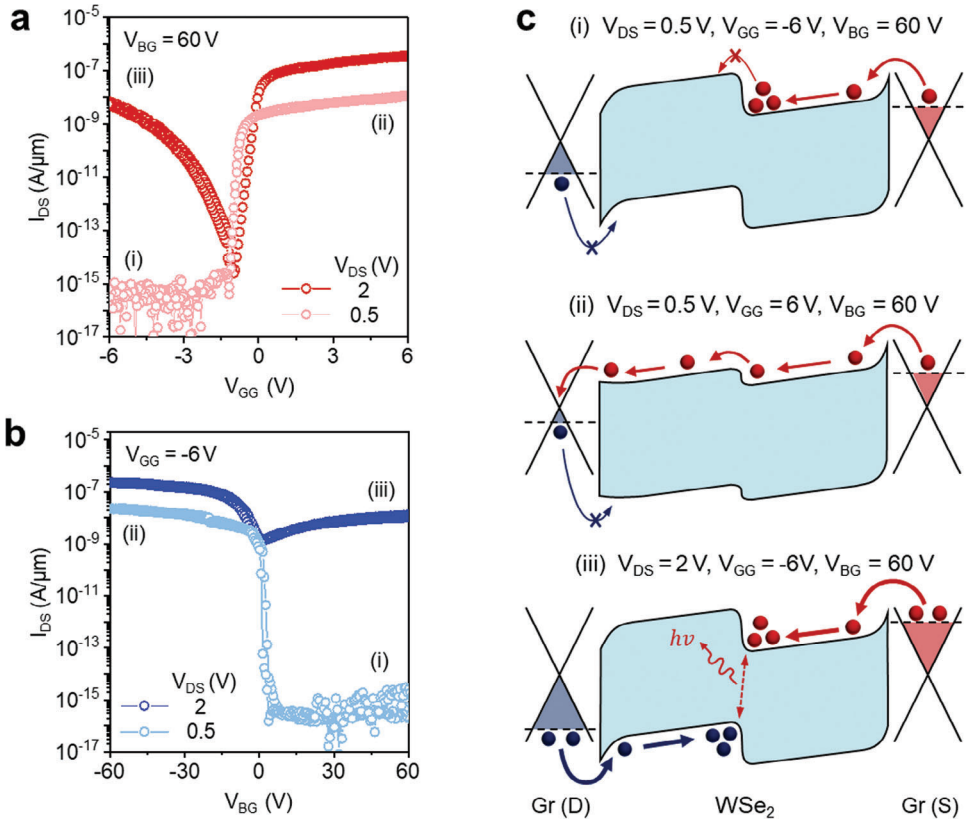


**Figure 2.** Reconfigurable transport properties using electrical modulation of $WSe_2$ LET. a) Transfer curve ($I_{DS}$–$V_{GG}$) of the device at a fixed voltage of $V_{BG}$ = 60V for n-type transport operation. b) Transfer curve ($I_{DS}$–$V_{BG}$) of the device at a fixed voltage of $V_{GG}$ = −6V for p-type transport operation. c) Schematics of band diagrams of three conditions at the n-type operation of the device using electrical modulation. By adjusting the double gate and drain voltages, the carrier type injected into $WSe_2$ can be selected, and the carrier transport can be switched by modulating the potential barrier at the $WSe_2$ homojunction.

Supporting Information). It is worth noting that the monochromic EL peaks in the contour plots of Figure 4a,c were consistently maintained at 1.65 eV, regardless of applied bias and gate voltages. It is because the EL of the $WSe_2$ LETs occurs by e–h recombination through the intrinsic direct bandgap of $WSe_2$. At fixed $V_{GG}$ = −8 V which observed the highest EQE in Figure S10 (Supporting Information), the EQE of the $WSe_2$ LET extracted by varying the $V_{BG}$ increased as a function of the $V_{BG}$, reaching a maximum EQE of ≈8.2% at room temperature, as shown in Figure 4d. At the larger $V_{BG}$, the EQE slightly decreased along with the saturation of EL intensity, which indicates that balanced concentrations of electrons and holes are required for high light emission efficiency. We measured the EQEs of several $WSe_2$ LETs, where flux-grown and purchased samples of $WSe_2$ were used. The flux-grown $WSe_2$ showed higher EQEs than the purchased one, which is in agreement with the higher PL efficiency of the flux-grown samples (Figure S11, Supporting Information).[35]

**Figure** 5a,b shows the PL and EL spectra of the $WSe_2$ LET. All spectra can be deconvoluted into two peaks of neutral exciton ($X^0$) and charged exciton ($X^*$). When the $WSe_2$ LET was partially p- and n-doped by applying $V_{GG}$ = −6V and $V_{BG}$ = 60V as shown in the inset of Figure 5a, the PL spectra of these regions exhibited two dominant PL peaks corresponding to $X^*$ and $X^0$. Notably, the $X^*$ peak is stronger than the $X^0$ peak for both p- and n-doped regions. In contrast, $X^0$ is more dominant than $X^*$ in the EL spectrum of Figure 5b. As shown in Figure 5c, the EL intensity ratio of the neutral excitons to charged excitons ($X^0/X^*$) is 14 times higher than PL intensity ratios of $X^0/X^*$ in p- and n-doped regions. As shown in the schematic device geometry and energy band diagram of Figure 5d, the injected electrons and holes from n- and p-doped regions form exciton complexes at the 1D region. Notably, the in-plane electric field within the 1D region leads to the confinement of neutral excitons.[41] To investigate the effect of in-plane field and doping on the exciton behaviors, we calculated charge densities of electrons and holes, and potentials of neutral excitons and charged excitons ($X^+$ and $X^-$) using the electrostatic simulation of the device as shown in Figure 5e (See Experimental Section and Note S2, Supporting Information). The local doping by graphene and Si gates dopes the $WSe_2$ separately into adjacent p- and n-doped regions with large charge densities and in-plane electric field along the edge of graphene gate.[40] The in-plane electric field confines neutral excitons at the 1D nanoscale region of $WSe_2$ with minimum exciton potential. In addition, neutral excitons are pushed toward the 1D region by repulsive interaction that is caused by the charge density gradient.[41] This unique phenomenon is mainly observed in the ultrathin TMDs with large exciton binding energies, enabling excitons to withstand the

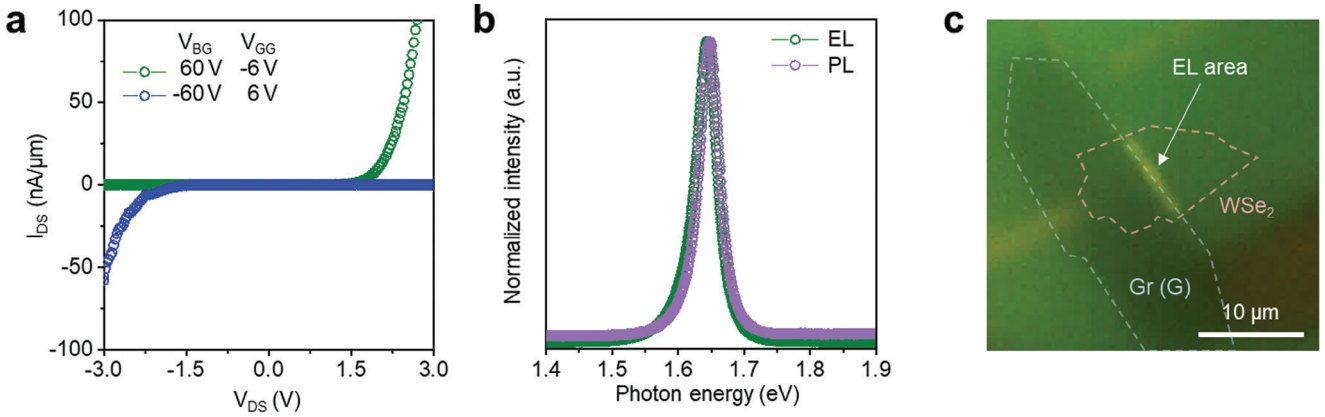


**Figure 3.** Light emission of $WSe_2$ LET. a) Output curves ($I_{DS}$–$V_{DS}$) at opposite voltage using double gates. The output curves show a rectifying behavior due to the p–n junction formation at $WSe_2$. b) Normalized PL and EL spectra of the device. The EL spectrum is consistent with the PL spectrum, which indicates that EL originated from e–h recombination across the direct bandgap of $WSe_2$. c) Optical image of light emission of the device. Strong EL is observed at the p–n junction of $WSe_2$.

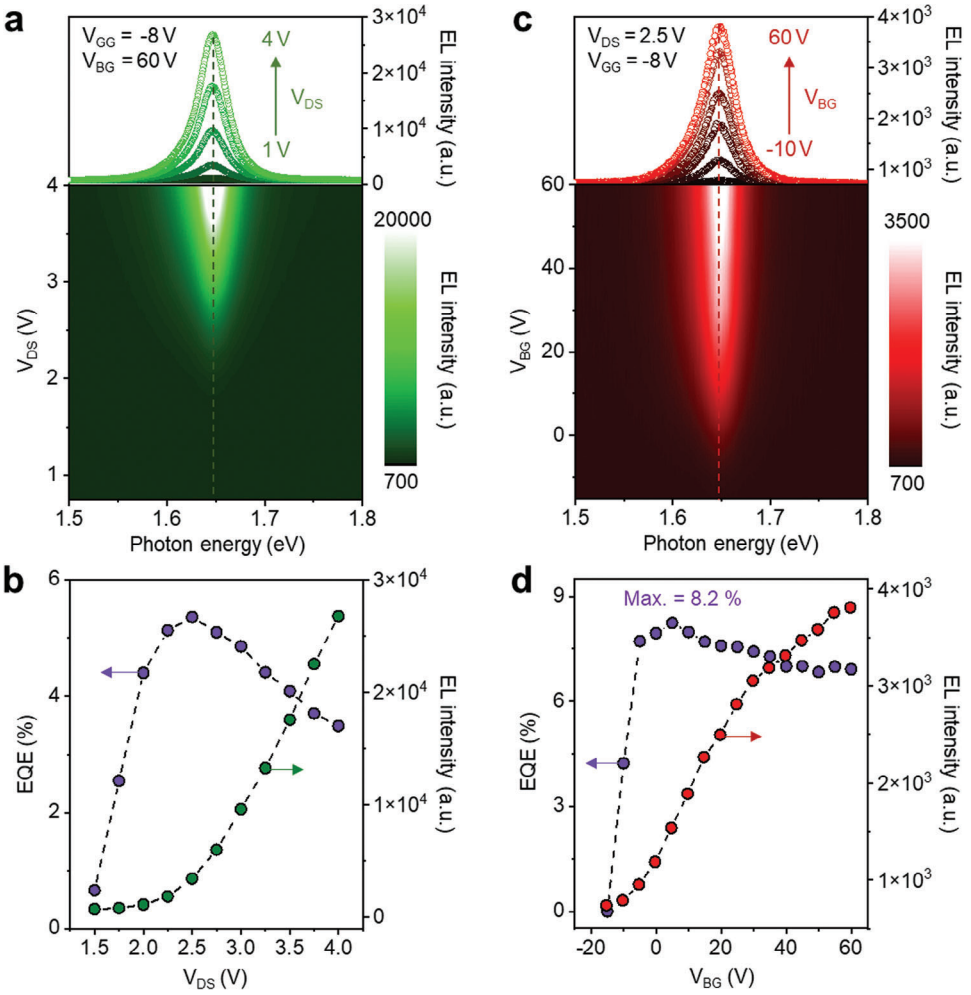


**Figure 4.** Electrical tunability of electroluminescence of $WSe_2$ LET. a) EL spectrum and contour plot of the device at varying $V_{DS}$ and fixed $V_{GG} = -8$V and $V_{BG} = 60$V. b) EQE (purple) and EL intensity (green) as a function of $V_{DS}$. $V_{GG}$ and $V_{BG}$ were fixed at −8 and 60V, respectively. c) EL spectrum and contour plot of the device at varying $V_{BG}$ and fixed $V_{DS} = 2.5$V and $V_{GG} = -8$V. d) EQE (purple) and EL intensity (red) as a function of $V_{BG}$. $V_{DS}$ and $V_{GG}$ were fixed at 2.5 and −8V, respectively. By optimizing with $V_{DS}$, $V_{BG}$, and $V_{GG}$, a maximum EQE of 8.2% was obtained with $WSe_2$ LET and EL intensity exhibits no peak shift.

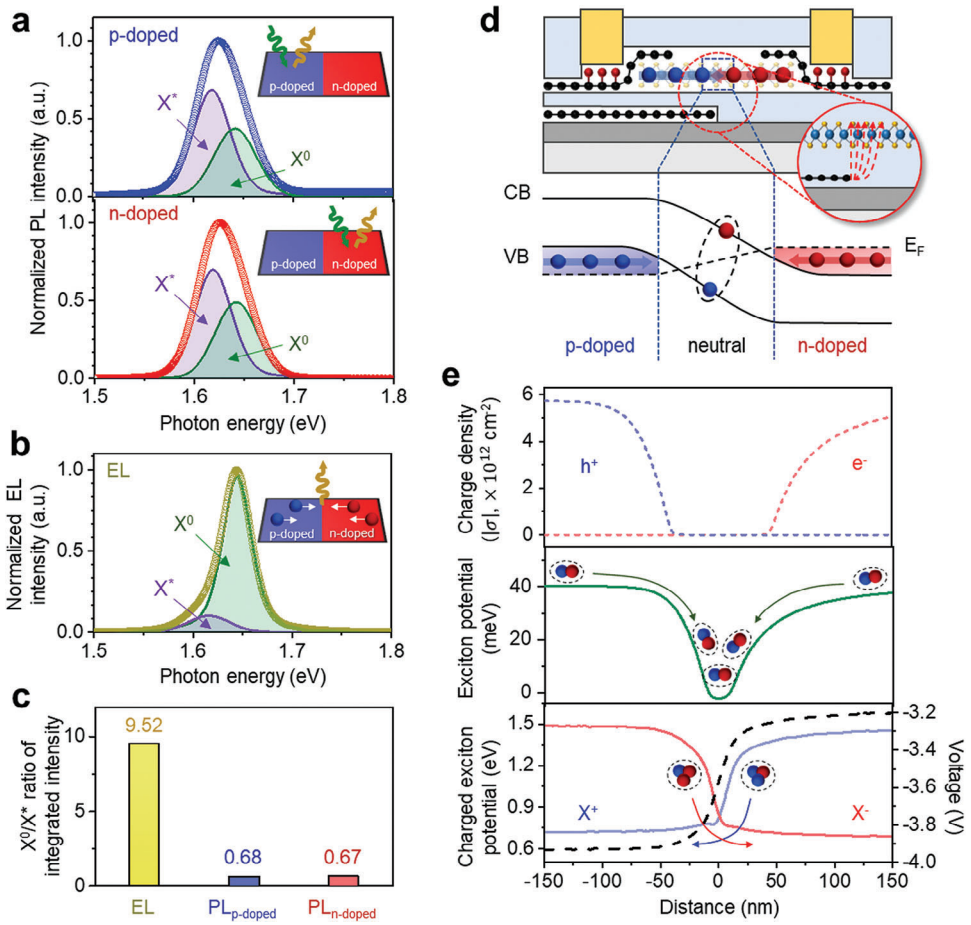


**Figure 5.** Electroluminescence of electrically confined neutral exciton at the 1D region in the p–n junction of $WSe_2$. a) Normalized PL spectrum of hole-doped (blue) and electron-doped (red) $WSe_2$ in the $WSe_2$ LET measured at $V_{GG} = -6V$ and $V_{BG} = 60V$, respectively. b) Normalized EL spectrum of the device. All spectrums were deconvoluted into the two distinct peaks of the neutral exciton ($X^0$, green) and charged exciton ($X^*$, purple). c) Comparison of $X^0/X^*$ ratio of integrated intensity in PL and EL. Compared to PL, the EL intensity of the device primarily arises from the neutral exciton. d) Schematic of the device structure and energy band diagram in $WSe_2$ LET. e) Electrostatic simulation of the spatial dependence of charge density of holes (blue dashed line) and electrons (red dashed line), exciton potential (green line), and potential of the positively charged exciton (blue line) and negatively charged exciton (red line), and voltage (black dashed line) in $WSe_2$. Since neutral excitons are electrically confined to the 1D region in $WSe_2$ and charged excitons are pushed away from the 1D region by the potential difference, $WSe_2$ LET can emit predominantly neutral excitons.

in-plane electric fields.[42] Furthermore, the charged excitons drift away from the 1D region by potential gradients of charged excitons (bottom of Figure 5e).[43,44] As a result, the EL from neutral excitons is predominant owing to their electrical confinement in the 1D region of $WSe_2$ LETs.

## 3. Conclusion

In conclusion, we demonstrate the efficient light-emitting devices based on monolayer $WSe_2$ that satisfy the prerequisites for high EQE: efficient injection of charge carriers and predominant emission of neutral excitons. Through precise band alignment of $WSe_2$ and graphene, and double gate geometry, the $WSe_2$ LETs can achieve efficient charge injection and e–h recombination for strong EL with a high EQE of ≈8.2%. Our results show that the strong EL peak of $WSe_2$ LET is attributed to the electrical confinement of neutral excitons due to the in-plane electric field and strong charge interactions. Our work not only highlights the potential of 2D light-emitting devices but also provides a new avenue for modulating the recombination of neutral and charged excitons for excitonic devices.

## 4. Experimental Section

*Device Fabrication*: All the flakes were mechanically exfoliated from a bulk crystal onto a $SiO_2$/Si substrate with a thickness of 285 nm of $SiO_2$. Two types of $WSe_2$ crystals were used, one grown by the self-flux method and the other purchased from SPI Supplies. A stack of flakes consisting of top hBN, graphene electrodes, $WSe_2$, and bottom hBN was fabricated using the pick-up transfer technique with a polydimethylsiloxane (PDMS) stamp coated with a polycarbonate (PC) film.[29] The stacked heterostructure was transferred onto graphene as a gate on a $SiO_2$ (285 nm)/Si substrate by releasing the PC film from the PDMS at 180 °C. The PC film was dissolved in chloroform overnight. The stacked heterostructure was annealed at 300 °C for 3 h in a $10^{-4}$ Torr vacuum to enhance adhesion between layers.[36] To form connections between the metal and embedded graphene, the sample was patterned using e-beam lithography (Raith

pioneer 2) and then it was exposed to $XeF_2$ gas of 2 Torr for 200 s at room temperature using $XeF_2$ etcher (VPE-4F, SAMCO).[37] The metals Cr (1 nm)/Pd (40 nm)/Au (50 nm) were deposited by an e-beam evaporator (Korea Vacuum Tech.) under ultrahigh vacuum conditions of $\approx 10^{-7}$ Torr, followed by a lift-off process.

*Raman and PL Measurements*: Raman and PL spectra were measured using Raman spectroscopy (LabRAM HR Evolution) with 532 nm laser excitation under ambient conditions. To obtain Raman and photoluminescence mapping images, samples were scanned on an *x*–*y* stage with laser illumination.

*Electrical and Optoelectrical Measurements*: For electrical measurement, a semiconductor parameter analyzer (Keithley 4200A-SCS) was used at room temperature under $10^{-3}$ Torr. EL spectra were measured using a customized optical measurement system with a photodetector (Si avalanche), and electrical bias and gate voltage were applied by source meters (Keithley 2400). All EL measurements were performed in a $10^{-2}$ Torr vacuum chamber, with light signals collected through ×100 objective lens. The use of vacuums enabled stable measurement of the devices.

*Electrostatic Simulation for Electrical Confinement of Exciton Complexes*: To obtain quantitative information on the in-plane electric field, charge density distributions, voltage, and excitonic confining potential of exciton and charged excitons in the device, commercial finite element analysis software (COMSOL Multiphysics) was used. The simulated device geometry is depicted in Figure 5, including double gates of graphene gate and silicon back gate, 1L graphene electrodes, and hBN with 30 nm thickness. The semiconductor behavior of $WSe_2$ was calculated using the drift-diffusion model with the density-gradient theory.[45] The carrier density was determined based on the Fermi–Dirac distribution, considering the band structure, Fermi level, and density of states (DOS) of $WSe_2$. The following material parameters were used in the calculation: bandgap of $WSe_2$ = 1.65 eV, dielectric constant = 21, carrier mobility = 31 $cm^2\ V^{-1}\ s^{-1}$, election affinity = 3.7 eV, effective DOS = $6 \times 10^{24}\ m^{-3}$. The dielectric constants for hBN were 3.76 and 6.93 along the out-of-plane and in-plane directions, respectively.[45–51] The excitonic confining potential was calculated using an equation derived from the previous studies, based on electric field and charge density obtained from calculation and measurement constants.[41] The constants used in this calculation were exciton polarizability ($10.027 \times 10^{-5}$ meV $cm^2\ kV^{-2}$), trion polarizability ($411.367 \times 10^{-5}$ meV $cm^2\ kV^{-2}$), trion hyperpolarizability ($8.48 \times 10^{-7}$ meV $cm^4\ kV^{-4}$), effective exciton–electron coupling strength (≈0.7 μeV $\mu m^2$), and trion–electron coupling strength (1.32 μeV $\mu m^2$).[52–54]

## Supporting Information

Supporting Information is available from the Wiley Online Library or from the author.

## Acknowledgements

J.-C.S. and J.H.J. contributed equally to this work. This work was supported by the LG Display and the National Research Foundation of Korea (NRF) Grant funded by the Korean Government (2021R1A2C3014316 and 2017R1A5A1014862 (SRC program: vdWMRC center)). G.H.L. acknowledges the support from the Research Institute of Advanced Materials (RIAM), the Institute of Engineering Research (IER), the Institute of Applied Physics (IAP), and the Inter-University Semiconductor Research Center (ISRC) at the Seoul National University. M.C and Y.D.K were supported by NRF of Korea, (2022R1A4A3030766, 2021R1A2C2093155, and 2021R1A6C101A437). K.W. and T.T. acknowledge support from the JSPS KAKENHI (Grant Numbers 21H05233 and 23H02052) and the World Premier International Research Center Initiative (WPI), MEXT, Japan.

## Conflict of Interest

The authors declare no conflict of interest.

## Data Availability Statement

The data that support the findings of this study are available from the corresponding author upon reasonable request.

## Keywords

electrical confinement, electroluminescence, light-emitting transistor, neutral exciton, van der Waals heterostructure

Received: October 10, 2023
Revised: December 29, 2023
Published online:

[1] K. F. Mak, J. Shan, *Nat. Photonics* **2016**, *10*, 216.
[2] T. Mueller, E. Malic, *npj 2D Mater. Appl.* **2018**, *2*, 29.
[3] Q. H. Wang, K. Kalantar-Zadeh, A. Kis, J. N. Coleman, M. S. Strano, *Nat. Nanotechnol.* **2012**, *7*, 699.
[4] A. Chernikov, T. C. Berkelbach, H. M. Hill, A. Rigosi, Y. Li, B. Aslan, D. R. Reichman, M. S. Hybertsen, T. F. Heinz, *Phys. Rev. Lett.* **2014**, *113*, 076802.
[5] L. Britnell, R. M. Ribeiro, A. Eckmann, R. Jalil, B. D. Belle, A. Mishchenko, Y.-J. Kim, R. V. Gorbachev, T. Georgiou, S. V. Morozov, A. N. Grigorenko, A. K. Geim, C. Casiraghi, A. H. C. Neto, K. S. Novoselov, *Science* **2013**, *340*, 1311.
[6] D.-H. Lien, S. Z. Uddin, M. Yeh, M. Amani, H. Kim, J. W. Ager, E. Yablonovitch, A. Javey, *Science* **2019**, *364*, 468.
[7] H. Kim, S. Z. Uddin, N. Higashitarumizu, E. Rabani, A. Javey, *Science* **2021**, *373*, 448.
[8] Y. J. Zhang, T. Oka, R. Suzuki, J. T. Ye, Y. Iwasa, *Science* **2014**, *344*, 725.
[9] K. F. Mak, K. He, C. Lee, G. H. Lee, J. Hone, T. F. Heinz, J. Shan, *Nat. Mater.* **2013**, *12*, 207.
[10] H. Ryu, J. Kwon, S. Yang, K. Watanabe, T. Taniguchi, Y. D. Kim, J. Hone, C.-H. Lee, G.-H. Lee, *ACS Photonics* **2021**, *8*, 3455.
[11] Z. Wang, D. A. Rhodes, K. Watanabe, T. Taniguchi, J. C. Hone, J. Shan, K. F. Mak, *Nature* **2019**, *574*, 76.
[12] X.-X. Zhang, Y. You, S. Y. F. Zhao, T. F. Heinz, *Phys. Rev. Lett.* **2015**, *115*, 257403.
[13] J. Wang, I. Verzhbitskiy, G. Eda, *Adv. Mater.* **2018**, *30*, 1802687.
[14] A. Pospischil, M. M. Furchi, T. Mueller, *Nat. Nanotechnol.* **2014**, *9*, 257.
[15] J. S. Ross, P. Klement, A. M. Jones, N. J. Ghimire, J. Yan, D. G. Mandrus, T. Taniguchi, K. Watanabe, K. Kitamura, W. Yao, D. H. Cobden, X. Xu, *Nat. Nanotechnol.* **2014**, *9*, 268.
[16] B. W. H. Baugher, H. O. H. Churchill, Y. Yang, P. Jarillo-Herrero, *Nat. Nanotechnol.* **2014**, *9*, 262.
[17] F. Withers, O. Del Pozo-Zamudio, A. Mishchenko, A. P. Rooney, A. Gholinia, K. Watanabe, T. Taniguchi, S. J. Haigh, A. K. Geim, A. I. Tartakovskii, K. S. Novoselov, *Nat. Mater.* **2015**, *14*, 301.
[18] D.-H. Lien, M. Amani, S. B. Desai, G. H. Ahn, K. Han, J.-H. He, J. W. Ager, M. C. Wu, A. Javey, *Nat. Commun.* **2018**, *9*, 1229.
[19] T. Ahmed, J. Zha, K. K. Lin, H.-C. Kuo, C. Tan, D.-H. Lien, *Adv. Mater.* **2023**, *35*, 2208054.
[20] J. Kwon, J.-C. Shin, H. Ryu, J. Y. Lee, D. Seo, K. Watanabe, T. Taniguchi, Y. D. Kim, J. Hone, C.-H. Lee, G.-H. Lee, *Adv. Mater.* **2020**, *32*, 2003567.
[21] J. Zaumseil, R. H. Friend, H. Sirringhaus, *Nat. Mater.* **2006**, *5*, 69.
[22] S. Z. Bisri, T. Takenobu, K. Sawabe, S. Tsuda, Y. Yomogida, T. Yamao, S. Hotta, C. Adachi, Y. Iwasa, *Adv. Mater.* **2011**, *23*, 2753.
[23] J. S. Ross, S. Wu, H. Yu, N. J. Ghimire, A. M. Jones, G. Aivazian, J. Yan, D. G. Mandrus, D. Xiao, W. Yao, X. Xu, *Nat. Commun.* **2013**, *4*, 1474.

[24] A. Allain, A. Kis, *ACS Nano* **2014**, *8*, 7180.
[25] F. Withers, O. Del Pozo-Zamudio, S. Schwarz, S. Dufferwiel, P. M. Walker, T. Godde, A. P. Rooney, A. Gholinia, C. R. Woods, P. Blake, S. J. Haigh, K. Watanabe, T. Taniguchi, I. L. Aleiner, A. K. Geim, V. I. Fal'ko, A. I. Tartakovskii, K. S. Novoselov, *Nano Lett.* **2015**, *15*, 8223.
[26] K. Wu, H. Ma, Y. Gao, W. Hu, J. Yang, *J. Mater. Chem. A* **2019**, *7*, 7430.
[27] G.-H. Lee, X. Cui, Y. D. Kim, G. Arefe, X. Zhang, C.-H. Lee, F. Ye, K. Watanabe, T. Taniguchi, P. Kim, J. Hone, *ACS Nano* **2015**, *9*, 7019.
[28] Y.-J. Yu, Y. Zhao, S. Ryu, L. E. Brus, K. S. Kim, P. Kim, *Nano Lett.* **2009**, *9*, 3430.
[29] P. J. Zomer, M. H. D. Guimarães, J. C. Brant, N. Tombros, B. J. Van Wees, *Appl. Phys. Lett.* **2014**, *105*, 013101.
[30] J.-C. Shin, Y. H. Kim, K. Watanabe, T. Taniguchi, C.-H. Lee, G.-H. Lee, *Adv. Mater. Interfaces* **2022**, *9*, 2101763.
[31] H. Fang, S. Chuang, T. C. Chang, K. Takei, T. Takahashi, A. Javey, *Nano Lett.* **2012**, *12*, 3788.
[32] R. Decker, Y. Wang, V. W. Brar, W. Regan, H.-Z. Tsai, Q. Wu, W. Gannett, A. Zettl, M. F. Crommie, *Nano Lett.* **2011**, *11*, 2291.
[33] C. R. Dean, A. F. Young, I. Meric, C. Lee, L. Wang, S. Sorgenfrei, K. Watanabe, T. Taniguchi, P. Kim, K. L. Shepard, J. Hone, *Nat. Nanotechnol.* **2010**, *5*, 722.
[34] J. Wierzbowski, J. Klein, F. Sigger, C. Straubinger, M. Kremser, T. Taniguchi, K. Watanabe, U. Wurstbauer, A. W. Holleitner, M. Kaniber, K. Müller, J. J. Finley, *Sci. Rep.* **2017**, *7*, 12383.
[35] D. Edelberg, D. Rhodes, A. Kerelsky, B. Kim, J. Wang, A. Zangiabadi, C. Kim, A. Abhinandan, J. Ardelean, M. Scully, D. Scullion, L. Embon, R. Zu, E. J. G. Santos, L. Balicas, C. Marianetti, K. Barmak, X. Zhu, J. Hone, A. N. Pasupathy, *Nano Lett.* **2019**, *19*, 4371.
[36] H. Rokni, W. Lu, *Nat. Commun.* **2020**, *11*, 5607.
[37] J. Son, J. Kwon, S. Kim, Y. Lv, J. Yu, J.-Y. Lee, H. Ryu, K. Watanabe, T. Taniguchi, R. Garrido-Menacho, N. Mason, E. Ertekin, P. Y. Huang, G.-H. Lee, A. M. Van Der Zande, *Nat. Commun.* **2018**, *9*, 3988.
[38] Y. Shin, J. Kwon, Y. Jeong, K. Watanabe, T. Taniguchi, S. Im, G.-H. Lee, *Small* **2022**, *18*, 2200882.
[39] X. Cui, G.-H. Lee, Y. D. Kim, G. Arefe, P. Y. Huang, C.-H. Lee, D. A. Chenet, X. Zhang, L. Wang, F. Ye, F. Pizzocchero, B. S. Jessen, K. Watanabe, T. Taniguchi, D. A. Muller, T. Low, P. Kim, J. Hone, *Nat. Nanotechnol.* **2015**, *10*, 534.
[40] M. Massicotte, F. Vialla, P. Schmidt, M. B. Lundeberg, S. Latini, S. Haastrup, M. Danovich, D. Davydovskaya, K. Watanabe, T. Taniguchi, V. I. Fal'ko, K. S. Thygesen, T. G. Pedersen, F. H. L. Koppens, *Nat. Commun.* **2018**, *9*, 1633.
[41] D. Thureja, A. Imamoglu, T. Smolenski, I. Amelio, A. Popert, T. Chervy, X. Lu, S. Liu, K. Barmak, K. Watanabe, T. Taniguchi, D. J. Norris, M. Kroner, P. A. Murthy, *Nature* **2022**, *606*, 298.
[42] M. Goryca, J. Li, A. V. Stier, T. Taniguchi, K. Watanabe, E. Courtade, S. Shree, C. Robert, B. Urbaszek, X. Marie, S. A. Crooker, *Nat. Commun.* **2019**, *10*, 4172.
[43] L. A. Jauregui, A. Y. Joe, K. Pistunova, D. S. Wild, A. A. High, Y. Zhou, G. Scuri, K. De Greve, A. Sushko, C.-H. Yu, T. Taniguchi, K. Watanabe, D. J. Needleman, M. D. Lukin, H. Park, P. Kim, *Science* **2019**, *366*, 870.
[44] D. Sanvitto, F. Pulizzi, A. J. Shields, P. C. M. Christianen, S. N. Holmes, M. Y. Simmons, D. A. Ritchie, J. C. Maan, M. Pepper, *Science* **2001**, *294*, 837.
[45] M. G. Ancona, *J Comput Electron* **2011**, *10*, 65.
[46] S.-Y. Lee, T.-Y. Jeong, J.-H. Kim, S. Yun, K.-J. Yee, *Opt. Express* **2018**, *26*, 23061.
[47] W. Zhao, Z. Ghorannevis, L. Chu, M. Toh, C. Kloc, P.-H. Tan, G. Eda, *ACS Nano* **2013**, *7*, 791.
[48] B. Liu, Y. Ma, A. Zhang, L. Chen, A. N. Abbas, Y. Liu, C. Shen, H. Wan, C. Zhou, *ACS Nano* **2016**, *10*, 5153.
[49] Y. Liang, S. Huang, R. Soklaski, L. Yang, *Appl. Phys. Lett.* **2013**, *103*, 042106.
[50] P. R. Patel, J. R. Rathod, H. S. Patel, K. D. Patel, V. M. Pathak, *Adv. Mater. Res.* **2013**, *665*, 53.
[51] A. Laturia, M. L. Van De Put, W. G. Vandenberghe, *npj 2D Mater. Appl.* **2018**, *2*, 6.
[52] L. S. R. Cavalcante, D. R. Da Costa, G. A. Farias, D. R. Reichman, A. Chaves, *Phys Rev B* **2018**, *98*, 245309.
[53] Y. Xu, C. Horn, J. Zhu, Y. Tang, L. Ma, L. Li, S. Liu, K. Watanabe, T. Taniguchi, J. C. Hone, J. Shan, K. F. Mak, *Nat. Mater.* **2021**, *20*, 645.
[54] E. Liu, J. Van Baren, Z. Lu, M. M. Altaiary, T. Taniguchi, K. Watanabe, D. Smirnov, C. H. Lui, *Phys. Rev. Lett.* **2019**, *123*, 027401.